PHOTONICS Research

Hybrid-type white LEDs based on inorganic halide perovskite QDs: candidates for wide color gamut display backlights

Chih-Hao Lin,[1] Akta Verma,[2] Chieh-Yu Kang,[1] Yung-Min Pai,[1] Tzu-Yu Chen,[1] Jin-Jia Yang,[1] Chin-Wei Sher,[3] Ya-Zhu Yang,[4] Po-Tsung Lee,[1] Chien-Chung Lin,[5] Yu-Chuan Wu,[6,7] S. K. Sharma,[2] Tingzhu Wu,[8,9] Shu-Ru Chung,[4,10] and Hao-Chung Kuo[1,11]

[1]Department of Photonics and Institute of Electro-Optical Engineering, College of Electrical and Computer Engineering, Taiwan Chiao Tung University, Hsinchu 30010, China
[2]Department of Applied Physics, Indian Institute of Technology (Indian School of Mines), Dhanbad-826004, India
[3]Fok Ying Tung Research Institute, Hong Kong University of Science and Technology, Hong Kong, China
[4]Department of Materials Science and Engineering, Taiwan Formosa University, Yunlin 63201, China
[5]Institute of Photonic System, College of Photonics, Taiwan Chiao Tung University, Tainan 711, China
[6]Department of Materials and Mineral Resources Engineering, Taiwan Taipei University of Technology, Taipei 10608, China
[7]Department of Chemical and Materials Engineering, Chinese Culture University, Taipei 11114, China
[8]Department of Electronic Science, Fujian Engineering Research Center for Solid-state Lighting, Collaborative Innovation Center for Optoelectronic Semiconductors and Efficient Devices, Xiamen University, Xiamen 361005, China
[9]e-mail: wutingzhu@xmu.edu.cn
[10]e-mail: srchung@nfu.edu.tw
[11]e-mail: hckuo@faculty.nctu.edu.tw

Received 28 December 2018; revised 3 February 2019; accepted 11 March 2019; posted 14 March 2019 (Doc. ID 356364); published 30 April 2019

We demonstrate inorganic halide perovskite quantum-dots-based white light-emitting diodes via three different geometries, including liquid, solid, and hybrid types. Problems of fast anion exchange and aggregation in the cases of liquid- and solid-type devices are discussed in detail and push us to move towards the fabrication of a hybrid-type device structure. The experiment results illustrate that a hybrid-type device has the highest luminance efficiency (51 lm/W) and a wide color gamut (122% of NTSC and 91% of Rec. 2020). Therefore, we conclude that a hybrid-type device can provide an outstanding color gamut for high color gamut display applications.

https://doi.org/10.1364/PRJ.7.000579

1. INTRODUCTION

Recently, popularity of colloidal quantum dots (QDs) and their association in optoelectronic device applications such as light emitting diodes (LEDs), photovoltaics, and photo-detectors has increased rapidly [1–5]. For the past decade, LEDs have received great attention because of their energy-saving capability, in both the research community and industry [6–9]. Further, QDs are rising as excellent materials for white LED (WLED) applications because of their various unique properties such as broad absorption band, narrow emission peak, and wavelength-dependent size [3,10,11]. The main advantages of QD-based WLEDs over conventional WLEDs and organic LEDs (OLEDs) are high color purity with low cost production [12,13]. In addition to these properties, high quantum yields (QYs) and good spectral overlap show great potential towards improvement in the efficiency of WLEDs [14]. All these characteristics make QDs highly significant emerging candidates for the development of next-generation display technologies [15]. In 1994, Colvin *et al.* reported the first CdSe QDs-based LEDs [16]. In the last few years, halide perovskite QDs (PQDs) have been demonstrated as amazing semiconductors for lighting application [17,18]. Also, PQDs have potential to combine with flexible technology [19,20]. Recently, the Liu group reported the color gamut can be achieved at 113% of NTSC by using the halide PQDs [21]. However, PQDs still have problems in practical applications, such as instability, anion-exchange reaction, intrinsic QD surface oxidation, photo bleaching, and aggregation. The two major issues that limit practical applications are their instability and anion-exchange reaction when different halide PQDs mix together [22,23]. Hence, we attempt to enhance the performance for practical applications based on the target for improving the main issues. Recently, two-dimensional PQDs have attracted attention due to their superior stabilities as photovoltaic devices [24–26]. In display application, it is important to develop a suitable packaging type

to overcome the anion-exchange reaction in order to get long-term stability of PQDs.

By keeping this in mind, in the present context, three different device geometries were prepared, such as liquid (red and green PQDs), solid (green and red film), and hybrid types (green liquid and red film). In the current case, it was found that fast anion exchange occurs between green ($CsPbBr_3$) and red ($CsPbBr_{1.2}I_{1.8}$) light halide PQDs in liquid-type devices. As a result, only one photoluminescence (PL) peak is observable due to the dispersion of both halide PQDs. Moreover, in the case of the solid type, efficiency loss occurs due to the so-called self-aggregation effect [6,23]. Hence, efforts were continued further to develop hybrid-type devices. Finally, out of all these above-mentioned types, the hybrid-type scheme owns high efficiency (51 lm/W). Still, it suffers low efficiency; this may be due to the presence of resin in the solid case, and by using high external quantum efficiency (EQE) LEDs, efficiency can be improved. However, the best part of the present work is the outstanding color gamut that can reach 122% of NTSC standard and 91% of Rec. 2020 at a correlated color temperature (CCT) of 5516 K. The obtained NTSC and Rec. 2020 results are even higher than standard red, green, and blue chip values.

2. MATERIAL AND DEVICE FABRICATION

The inorganic green ($CsPbBr_3$) and red ($CsPbBr_{1.2}I_{1.8}$) light halide PQDs were synthesized by hot-injection methods in this study. A few grams of PbX_2 ($PbBr_2$ and PbI_2 with different weight ratios of different colors) and 10 mL octadecene (ODE) were loaded into a three-necked flask and vacuum dried at 120°C for 1 h. After that, oleylamine (OLA) and oleic acid (OA) were injected into the flask under Ar atmosphere and mixed until completely dissolved. Further, we raised the reaction temperature to 180°C and quickly injected the as-prepared Cs-oleate solution into the flask. After reacting for 5 s, the reaction mixture cooled down by ice-water bath to room temperature. Finally, the PQDs were centrifuged, the supernatant abandoned, and the particles re-dissolved into the solvent. In the device fabrication, the three types of structures were prepared in order to perform a comparison among liquid-, solid-, and hybrid-type WLEDs. Fig. 1 shows the schematic process for liquid-, solid- and hybrid-type device structures. In the case of a liquid-type device, first, we used a small glass cup with inner and outer radii of 5 mm and 6 mm, respectively. The cup was sealed by thin glass with size 1.3 cm × 1.3 cm. Finally, in this way, a glass box was assembled by pasting a thin glass on top of the glass box. Then a hole was created on the top surface with the help of a laser. After that, red and green PQDs were injected into the glass box, and it was sealed again with thin glass, as shown in Fig. 1(a). It is also important to mention here that fast anion exchange occurring in liquid-type devices motivates us to move towards other geometries. Hence, Fig. 1(b) illustrates the schematic diagram for solid-type PQDs device structure. Further, for preparing solid films, we first injected red and green PQDs separately into a glass box, and afterwards, the UV glue was added to it and then kept for 30 s under UV light of 365 nm wavelength for curing. Finally, we prepared a hybrid-type halide PQD structure, as shown in Fig. 1(c). For this, we first prepared a red PQD film by a similar procedure as mentioned above in the solid-type device structure. Afterwards, liquid green PQDs were poured into a glass box that was assembled by the same procedure as mentioned above in the liquid-type device case. Finally, in order to pump three types of devices, a 5070-packaging type blue LED with 450 nm was used. The blue LED chip was first fixed on the sub-mount. Also, the same halide PQDs and characterization were used throughout the liquid-, solid- and hybrid-type device fabrication. The different device structures were prepared to optimize the color gamut. The optical properties of the PQDs were measured by a UV-visible (UV-Vis) spectrometer (Hitachi UH5300) and a fluorescence (FL) spectrophotometer (FL, Hitachi F-7000). The concentrations of the PQDs and R6G dye were adjusted to the same optical density at the same excitation wavelength. Relative QYs were obtained by comparison with a standard R6G (QY 95%) in methanol. The QY of samples was calculated by the following equation [27]:

$$\mathrm{QY}_s = \frac{A_r F_r n_r^2}{A_s F_s n_s^2} \mathrm{QY}_r. \tag{1}$$

Here, F_s and F_r are the integrated FL emission areas of the sample and the reference. A_s and A_r are the absorbances at the same excitation wavelength of the sample and the reference, n_s and n_r are the solvent refractive indices of the sample and the reference, and QY_s and QY_r are the QY of the sample and the

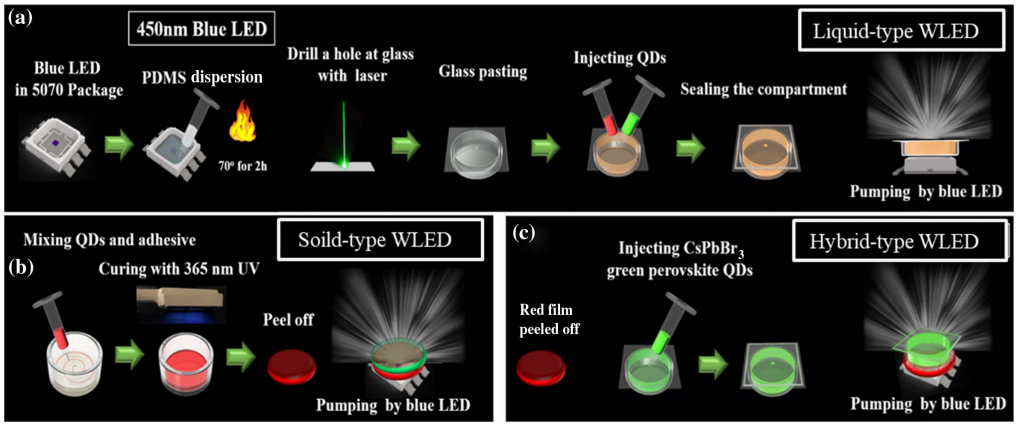

Fig. 1. Process flow of perovskite QDs-based WLEDs: (a) liquid type, (b) solid type, and (c) hybrid type.

reference, respectively. The full width at half maximum (FWHM) of the used PQDs is 19 nm and 33 nm for green and red, respectively. Further, both green and red PQDs possess PL QY as 147% and 30%, respectively. The integrating sphere (50 cm in diameter), spectrometer (resolution 0.5 nm, model CAS 140CT from Instrument System GmbH in Germany), power supplies (Agilent E3632A, Keithley 2400, and Motech DR2004), and computer with Isuzu Optics software were used to measure optical and electrical characteristics for all prepared three WLEDs devices. The thermal images for both solid and hybrid-type device structures were recorded by using Testo 875 having tunable lenses, with high-temperature measurement (up to 550°C) and convenient-to-use analysis software.

3. MEASUREMENT AND ANALYSIS

A. Liquid-Type LEDs

Figures 2(a) and 2(b) show the UV-Vis absorption spectrum and PL emission spectrum for both red and green PQDs, respectively. The PL emission spectra for both green and red PQDs were recorded at excitation wavelengths of 370 nm and 365 nm, respectively. The sharp absorption edge and PL emission peak are located at 505 nm and 520 nm in the case of green PQDs, respectively. For red PQDs, a broad absorption band is observable near 629 nm, and a sharp PL emission peak is centered at 640 nm. Further, Wang and Protesescu reported similar results for absorption and PL emission spectra of PQDs [21,28]. The insets in Figs. 2(a) and 2(b) show photographs of PQDs under UV light. Further, Fig. 2(c) represents the electroluminescence (EL) spectrum and schematic diagram for liquid-type device structure with a driving current of 10 mA. The EL spectrum consists of only two peaks: one centered at 450 nm and the other at 567 nm with the FWHM about 14 nm. The former one is due to the blue LED chip, while the latter is caused by fast anion exchange due to mixing the two colors (red and green) of halide PQDs [29]. Finally, only one emission peak appearing between red and green light can be observed after completion of anion exchange. It can be depicted from the obtained single peak that fast anion exchange occurs in between both PQDs simultaneously. As a result, the PL peak of $CsPbBr_3$ moves towards longer wavelength, and on the other side, $CsPbBr_{1.2}I_{1.8}$ shifts to shorter wavelength [22,30]. The time taken to reach full anion exchange is 25–30 min in the present case. Further, in order to solve the diffusion (fast anion exchange) issue, we put effort towards separating the green and red peaks by owning two different types of WLEDs structures named as solid- and hybrid-type devices. The whole structure process is mentioned in Figs. 1(b) and 1(c).

B. Solid-Type and Hybrid-Type LEDs

Figures 3(a) and 3(b) represent the EL spectrum and color gamut of solid-type WLEDs, respectively. The spectrum contains three peaks located at 450 nm, 517 nm, and 622 nm corresponding to blue LEDs and green and red PQDs, respectively. Also, a little shift is observed in the case of red film due to the presence of iodine ions making $CsPbBr_{1.2}I_{1.8}$ unstable in time [31–33]. The inset in Fig. 3(a) shows the device structure of a solid-type WLED. The CCT and color coordinates are optimized at 5404 K and (0.33, 0.33), respectively. Figure 3(b) represents the color gamut that covers the wide area of NTSC (120%) and Rec. 2020 standards (90%). Although, the solid-type structure device showed good value for color gamut, it still was not highly efficient compared to the hybrid-type one. The reason behind reduction in efficiency depends mainly on packaging type [34]. Moreover, the aggregated QDs in solid type that are enclosed in silicone resin might cause scattering and re-absorption [3,35]. As a result, this would lead to efficiency loss. A few reports were found that suggested modification of silicone structure and dispersion of QDs might improve the efficiency of QDs LED. By keeping this motivation in mind, we further tried to improve luminance efficiency by owning another structure, i.e., hybrid type.

Figures 4(a) and 4(b) represent the EL spectrum and color gamut for hybrid-type WLEDs. The spectrum contains three peaks at the same position as mentioned above in the case of a solid-type WLED. The inset in Fig. 4(a) shows the device structure of hybrid type. In this device structure, we use red and green PQDs as a film and solution, respectively. The reason for choosing red PQDs as film is that the red PQDs are not stable in liquid form and the color changes to orange within a few weeks. Further, compared to liquid- and solid-type device structures, hybrid type has enhanced efficiency and wide color gamut. The CCT and color coordinates are optimized at 5516 K and (0.33, 0.34), respectively in this case. Figure 4(b) represents the color gamut that covers the wide area of 122% of NTSC and 91% of Rec. 2020 standards. From here, we believe

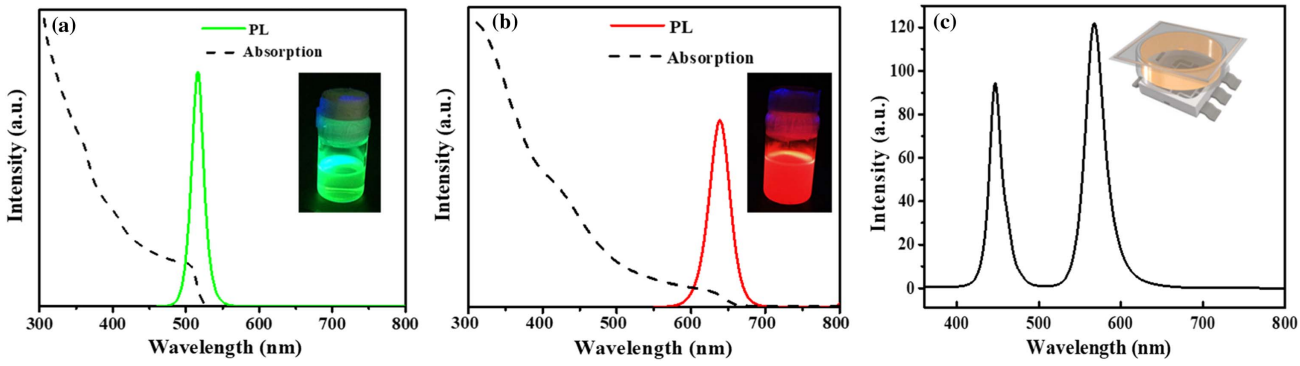

Fig. 2. UV–Vis absorption and PL emission spectrum of (a) $CsPbBr_3$ green and (b) $CsPbBr_{1.2}I_{1.8}$ red PQDs; the insets show photographs of green and red PQDs. (c) EL spectrum of liquid-type LEDs, which shows an intermediate stage due to mixing of red and green PQDs.

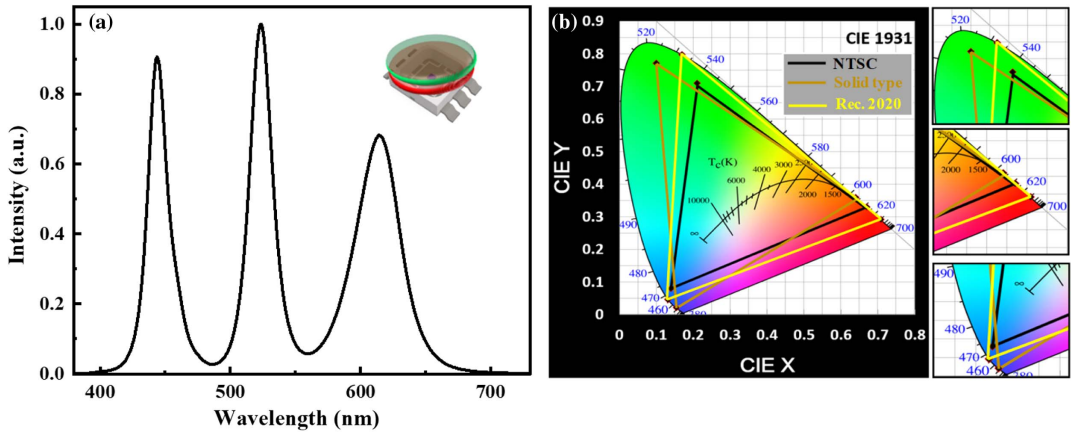

Fig. 3. (a) EL spectrum and (b) color gamut on CIE1931 for the solid-type WLED.

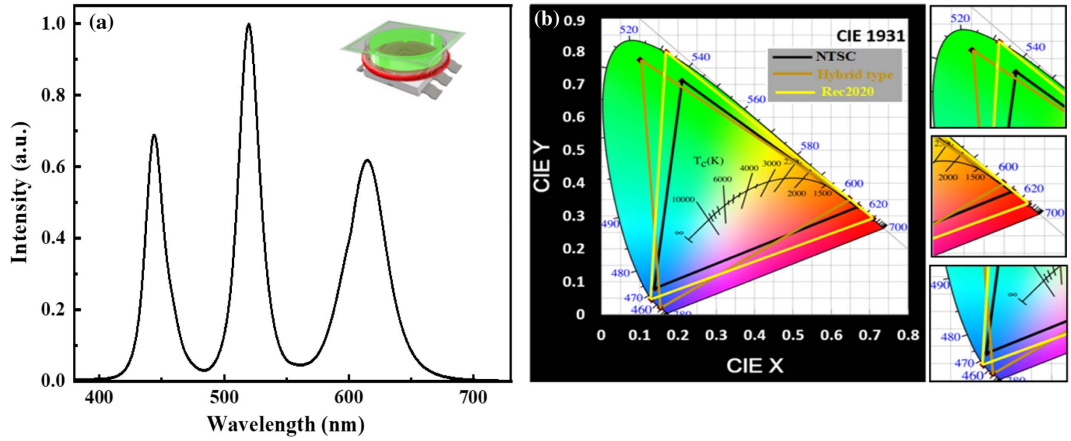

Fig. 4. (a) EL spectrum and (b) color gamut on CIE1931 for the hybrid-type WLED.

that the device structure will have great influence on performances of LEDs [36].

Figure 5 represents the current-dependent efficiency for solid- and hybrid-type devices. The efficiency of a hybrid-type device is found to be 51 lm/W, which is 24.5% higher than that of solid type, i.e., 41 lm/W. Here, the major concern in a solid-type device for efficiency loss is self-aggregation of QDs in the case of solid PQD films [37]. Further, the inset in Fig. 5 shows the current-dependent intensity comparison for both devices. On average, a hybrid-type device possesses higher stability than that of solid-type device structure.

Figure 6(a) shows the temperature versus current dependence for both devices. It is found that the temperature reached 78°C in the solid-type device at 250 mA. This high value of temperature on the surface is attributed to the non-radiative relaxation energy [38]. As a result, the device suffers reduction in efficiency and reliability. On the other hand, the hybrid-type device possesses low temperature on the surface, i.e., 40°C at 250 mA, which makes the device more reliable in performance and efficiency. Also, the glass sealed structure in the case of liquid-type QDs made it less influenced by thermal effect. Moreover, Figs. 6(b) and 6(c) represent thermal images for solid- and hybrid-type devices under a typical operating current of 100 mA with maximum surface temperatures of about 45°C and 32°C, respectively.

Figures 7(a) and 7(b) show the emission spectra of solid- and hybrid-type devices varying with time at room temperature

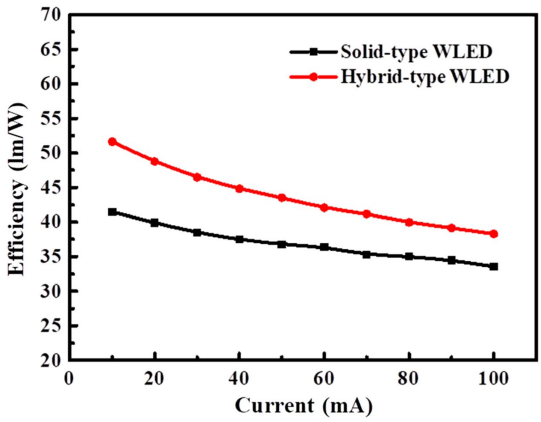

Fig. 5. Current versus luminance efficiency of solid- and hybrid-type WLEDs.

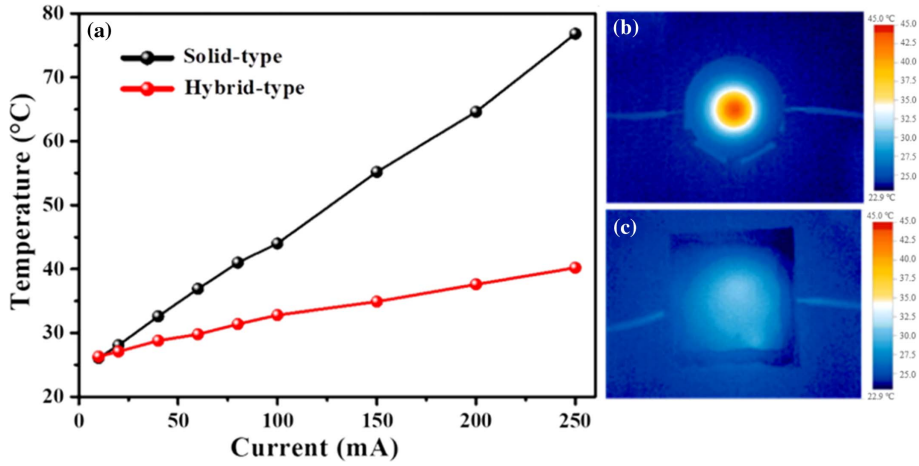

Fig. 6. Surface temperature images of WLED. (a) Temperature versus current plot for two different QDs devices. Thermal images for (b) solid type and (c) hybrid type at 100 mA.

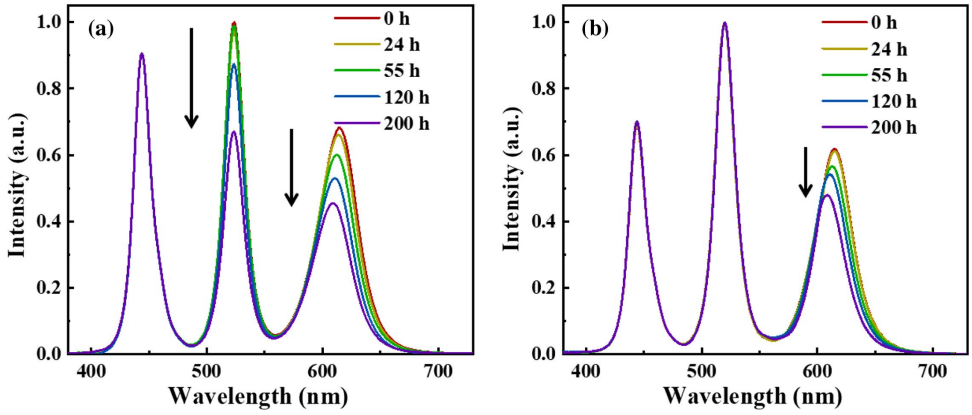

Fig. 7. Emission spectra of (a) solid-type and (b) hybrid-type WLEDs under various operation durations.

under 10 mA driven current. In the present case, the measurement time was set from 0 h to 200 h. Compared with spectra in Fig. 7(a), the liquid-type design for green perovskite improves the device's stability hugely in Fig. 7(b), but red perovskite still presents a slight intensity drop and color shift within solid film structure. For both solid-type and hybrid-type WLEDs, the areas of color gamut remain almost unchanged after 200 h aging. Area ratios of NTSC and Rec. 2020 reduce slightly from (120%, 90%) to (119%, 89%) for solid-type WLEDs, and from (122%, 91%) to (121%, 91%) for hybrid-type WLEDs after 200 h. The reason is that although the spectral intensity of solid-film QDs is attenuated, the spectral shape can almost remain the same.

It is found that luminance efficiency of a hybrid-type WLED decreases by only 12%, whereas it decreases by up to 28% for a solid-type WLED, as shown in Fig. 8. Normally, we set 30% intensity drop criteria to define LED package lifetime. Therefore, solid-type WLED's 30% decay's lifetime is close to only 200 h; it is obviously too short due to the unstable luminescent QDs and design. With this result, we can conclude that a hybrid-type device not only has high efficiency but also improves stability compared to solid-type design. Although we first proposed hybrid structure to solve red perovskite's anion exchange issue within a pure-liquid design WLED to reach ultra-high gamut result, we still need to improve this design's stability to meet real application criteria in future work.

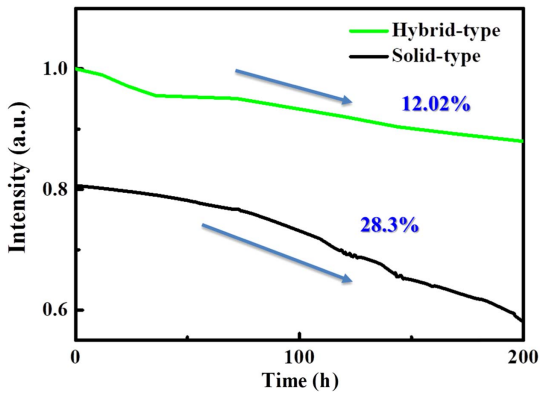

Fig. 8. Stability of solid- and hybrid-type WLEDs.

4. CONCLUSION

In summary, we have successfully fabricated high-luminance efficiency and a wide color gamut of PQDs-based solid and hybrid-type WLED devices. The hybrid-type device structure shows higher efficiency (51 lm/W) and outstanding wider color gamut (122% of NTSC and 91% of Rec. 2020 standards) values than that of a solid-type WLED. The finalized hybrid-type WLEDs possessing a decay rate of about 12% efficiency was found after operating for 200 h. Hence, the obtained results for the hybrid-type WLED device structure show great potential towards near-future high-color-quality display applications.

Funding. Ministry of Science and Technology, Taiwan (MOST), China (105-2221-E-009-112-MY3, 107-2221-E-009-113-MY3, 107-2221-E-009-114-MY3); Strait Postdoctoral Foundation of Fujian Province of China.

Acknowledgment. The authors would like to thank the Ministry of Science and Technology of Taiwan for its financial support, and express sincere gratitude to Lextar Corporation for helpful technical discussion and support. The authors declare that there are no conflicts of interest related to this article.

REFERENCES

1. A. Swarnkar, A. R. Marshall, E. M. Sanehira, B. D. Chernomordik, D. T. Moore, J. A. Christians, T. Chakrabarti, and J. M. Luther, "Quantum dot-induced phase stabilization of alpha-$CsPbI_3$ perovskite for high-efficiency photovoltaics," Science **354**, 92–95 (2016).
2. P. Martyniuk and A. Rogalski, "Quantum-dot infrared photodetectors: status and outlook," Prog. Quantum Electron. **32**, 89–120 (2008).
3. F. Fang, W. Chen, Y. Li, H. C. Liu, M. Mei, R. Zhang, J. J. Hao, M. Mikita, W. Q. Cao, R. K. Pan, K. Wang, and X. W. Sun, "Employing polar solvent controlled ionization in precursors for synthesis of high-quality inorganic perovskite nanocrystals at room temperature," Adv. Funct. Mater. **28**, 1706000 (2018).
4. B. Xie, H. C. Liu, R. Hu, C. F. Wang, J. J. Hao, K. Wang, and X. B. Luo, "Targeting cooling for quantum dots in white QDs-LEDs by hexagonal boron nitride platelets with electrostatic bonding," Adv. Funct. Mater. **28**, 1801407 (2018).
5. H. Y. Lin, C. W. Sher, D. H. Hsieh, X. Y. Chen, H. M. P. Chen, T. M. Chen, K. M. Lau, C. H. Chen, C. C. Lin, and H. C. Kuo, "Optical cross-talk reduction in a quantum-dot-based full-color micro-light-emitting-diode display by a lithographic-fabricated photoresist mold," Photon. Res. **5**, 411–416 (2017).
6. S. Nizamoglu and H. V. Demir, "Hybrid white light sources based on layer-by-layer assembly of nanocrystals on near-UV emitting diodes," Nanotechnology **18**, 405702 (2007).
7. K. J. Chen, H. C. Chen, K. A. Tsai, C. C. Lin, H. H. Tsai, S. H. Chien, B. S. Cheng, Y. J. Hsu, M. H. Shih, C. H. Tsai, H. H. Shih, and H. C. Kuo, "Resonant-enhanced full-color emission of quantum-dot-based display technology using a pulsed spray method," Adv. Funct. Mater. **22**, 5138–5143 (2012).
8. E. Jang, S. Jun, H. Jang, J. Llim, B. Kim, and Y. Kim, "White-light-emitting diodes with quantum dot color converters for display backlights," Adv. Mater. **22**, 3076–3080 (2010).
9. J. Ziegler, S. Xu, E. Kucur, F. Meister, M. Batentschuk, F. Gindele, and T. Nann, "Silica-coated InP/ZnS nanocrystals as converter material in white LEDs," Adv. Mater. **20**, 4068–4073 (2008).
10. P. Wang, X. Bai, C. Sun, X. Y. Zhang, T. Q. Zhang, and Y. Zhang, "Multicolor fluorescent light-emitting diodes based on cesium lead halide perovskite quantum dots," Appl. Phys. Lett. **109**, 063106 (2016).
11. X. L. Dai, Y. Z. Deng, X. G. Peng, and Y. Z. Jin, "Quantum-dot light-emitting diodes for large-area displays: towards the dawn of commercialization," Adv. Mater. **29**, 1607022 (2017).
12. Y. H. Kim, H. Cho, and T. W. Lee, "Metal halide perovskite light emitters," Proc. Natl. Acad. Sci. USA **113**, 11694–11702 (2016).
13. S. C. Hsu, L. A. Ke, H. C. Lin, T. M. Chen, H. Y. Lin, Y. Z. Chen, Y. L. Chueh, H. C. Kuo, and C. C. Lin, "Fabrication of a highly stable white light-emitting diode with multiple-layer colloidal quantum dots," IEEE J. Sel. Top. Quantum Electron. **23**, 2000109 (2017).
14. S. Sadeghi, B. G. Kumar, R. Melikov, M. M. Aria, H. B. Jalali, and S. Nizamoglu, "Quantum dot white LEDs with high luminous efficiency," Optica **5**, 793–802 (2018).
15. S. Demchyshyn, J. M. Roemer, H. Groiss, H. Heilbrunner, C. Ulbricht, D. Apaydin, A. Bohm, U. Rutt, F. Bertram, G. Hesser, M. C. Scharber, N. S. Sariciftci, B. Nickel, S. Bauer, E. D. Glowacki, and M. Kaltenbrunner, "Confining metal-halide perovskites in nanoporous thin films," Sci. Adv. **3**, e1700738 (2017).
16. V. L. Colvin, M. C. Schlamp, and A. P. Alivisatos, "Light-emitting-diodes made from cadmium selenide nanocrystals and a semiconducting polymer," Nature **370**, 354–357 (1994).
17. S. Ananthakumar, J. R. Kumar, and S. M. Babu, "Cesium lead halide ($CsPbX_3$, X = Cl, Br, I) perovskite quantum dots-synthesis, properties, and applications: a review of their present status," J. Photon. Energy **6**, 042001 (2016).
18. X. M. Li, Y. Wu, S. L. Zhang, B. Cai, Y. Gu, J. Z. Song, and H. B. Zeng, "$CsPbX_3$ quantum dots for lighting and displays: room-temperature synthesis, photoluminescence superiorities, underlying origins and white light-emitting diodes," Adv. Funct. Mater. **26**, 2435–2445 (2016).
19. P. K. Yang, Z. H. Lin, K. C. Pradel, L. Lin, X. H. Li, X. N. Wen, J. H. He, and Z. L. Wang, "Paper-based origami triboelectric nanogenerators and self-powered pressure sensors," ACS Nano **9**, 901–907 (2015).
20. P. K. Yang, L. Lin, F. Yi, X. H. Li, K. C. Pradel, Y. L. Zi, C. I. Wu, J. H. He, Y. Zhang, and Z. L. Wang, "A flexible, stretchable and shape-adaptive approach for versatile energy conversion and self-powered biomedical monitoring," Adv. Mater. **27**, 3817–3824 (2015).
21. H. C. Wang, S. Y. Lin, A. C. Tang, B. P. Singh, H. C. Tong, C. Y. Chen, Y. C. Lee, T. L. Tsai, and R. S. Liu, "Mesoporous silica particles integrated with all-inorganic $CsPbBr_3$ perovskite quantum-dot nanocomposites (MP-PQDs) with high stability and wide color gamut used for backlight display," Angew. Chem. **55**, 7924–7929 (2016).
22. G. Nedelcu, L. Protesescu, S. Yakunin, M. I. Bodnarchuk, M. J. Grotevent, and M. V. Kovalenko, "Fast anion-exchange in highly luminescent nanocrystals of cesium lead halide perovskites ($CsPbX_3$, X = Cl, Br, I)," Nano Lett. **15**, 5635–5640 (2015).
23. Q. A. Akkerman, V. D'Innocenzo, S. Accornero, A. Scarpellini, A. Petrozza, M. Prato, and L. Manna, "Tuning the optical properties of cesium lead halide perovskite nanocrystals by anion exchange reactions," J. Am. Chem. Soc. **137**, 10276–10281 (2015).
24. L. Dou, A. B. Wong, Y. Yu, M. Lai, N. Kornienko, S. W. Eaton, A. Fu, C. G. Bischak, J. Ma, T. Ding, N. S. Ginsberg, L.-W. Wang, A. P. Alivisatos, and P. Yang, "Atomically thin two-dimensional organic-inorganic hybrid perovskites," Science **349**, 1518–1521 (2015).
25. B. Cheng, T. Y. Li, P. C. Wei, J. Yin, K. T. Ho, J. R. D. Retamal, O. F. Mohammed, and J. H. He, "Layer-edge device of two-dimensional hybrid perovskites," Nat. Commun. **9**, 5196 (2018).
26. K. T. Ho, S. F. Leung, T. Y. Li, P. Maity, B. Cheng, H. C. Fu, O. F. Mohammed, and J. H. He, "Surface effect on 2D hybrid perovskite crystals: perovskites using an ethanolamine organic layer as an example," Adv. Mater. **30**, 1804372 (2018).
27. V. K. Ravi, R. A. Scheidt, A. Nag, M. Kuno, and P. V. Kamat, "To exchange or not to exchange. Suppressing anion exchange in cesium lead halide perovskites with $PbSO_4$-oleate capping," ACS Energy Lett. **3**, 1049–1055 (2018).
28. L. Protesescu, S. Yakunin, M. I. Bodnarchuk, F. Krieg, R. Caputo, C. H. Hendon, R. X. Yang, A. Walsh, and M. V. Kovalenko, "Nanocrystals of cesium lead halide perovskites ($CsPbX_3$, X = Cl, Br, and I): novel optoelectronic materials showing bright emission with wide color gamut," Nano Lett. **15**, 3692–3696 (2015).
29. S. J. Yoon, S. Draguta, J. S. Manser, O. Sharia, W. F. Schneider, M. Kuno, and P. V. Kamat, "Tracking iodide and bromide ion segregation in mixed halide lead perovskites during photoirradiation," ACS Energy Lett. **1**, 290–296 (2016).

30. H. C. Wang, Z. Bao, H. Y. Tsai, A. C. Tang, and R. S. Liu, "Perovskite quantum dots and their application in light-emitting diodes," Small **14**, 1702433 (2018).
31. H. Wang, N. Sui, X. Bai, Y. Zhang, Q. Rice, F. J. Seo, Q. B. Zhang, V. L. Colvin, and W. W. Yu, "Emission recovery and stability enhancement of inorganic perovskite quantum dots," J. Phys. Chem. Lett. **9**, 4166–4173 (2018).
32. H. Y. Tai, Y. H. Lin, and G. R. Lin, "Wavelength-shifted yellow electroluminescence of Si quantum-dot embedded 20-pair SiNx/SiOx superlattice by ostwald ripening effect," IEEE Photon. J. **5**, 6600110 (2013).
33. Z. G. Xiao, L. F. Zhao, N. L. Tran, Y. Lin, S. H. Silver, R. A. Kerner, N. Yao, A. Kahn, G. D. Scholes, and B. P. Rand, "Mixed-halide perovskites with stabilized bandgaps," Nano Lett. **17**, 6863–6869 (2017).
34. B. Xie, R. Hu, X. J. Yu, B. F. Shang, Y. P. Ma, and X. B. Luo, "Effect of packaging method on performance of light-emitting diodes with quantum dot phosphor," IEEE Photon. Technol. Lett. **28**, 1115–1118 (2016).
35. Y. Yuan, J. Zhang, G. L. Liang, and X. R. Yang, "Rapid fluorescent detection of neurogenin3 by CdTe quantum dot aggregation," Analyst **137**, 1775–1778 (2012).
36. C. W. Sher, C. H. Lin, H. Y. Lin, C. C. Lin, C. H. Huang, K. J. Chen, J. R. Li, K. Y. Wang, H. H. Tu, C. C. Fua, and H. C. Kuo, "A high quality liquid-type quantum dot white light-emitting diode," Nanoscale **8**, 1117–1122 (2016).
37. K. S. Cho, E. K. Lee, W. J. Joo, E. Jang, T. H. Kim, S. J. Lee, S. J. Kwon, J. Y. Han, B. K. Kim, B. L. Choi, and J. M. Kim, "High-performance crosslinked colloidal quantum-dot light-emitting diodes," Nat. Photonics **3**, 341–345 (2009).
38. H. Y. Lin, C. W. Sher, C. H. Lin, H. H. Tu, X. Y. Chen, Y. C. Lai, C. C. Lin, H. M. Chen, P. C. Yu, H. F. Meng, G. C. Chi, K. Honjo, T. M. Chen, and H. C. Kuo, "Fabrication of flexible white light-emitting diodes from photoluminescent polymer materials with excellent color quality," ACS Appl. Mater. Interfaces **9**, 35279–35286 (2017).